iScience

CellPress

Article

Nanostructured Three-Dimensional Percolative Channels for Separation of Oil-in-Water Emulsions

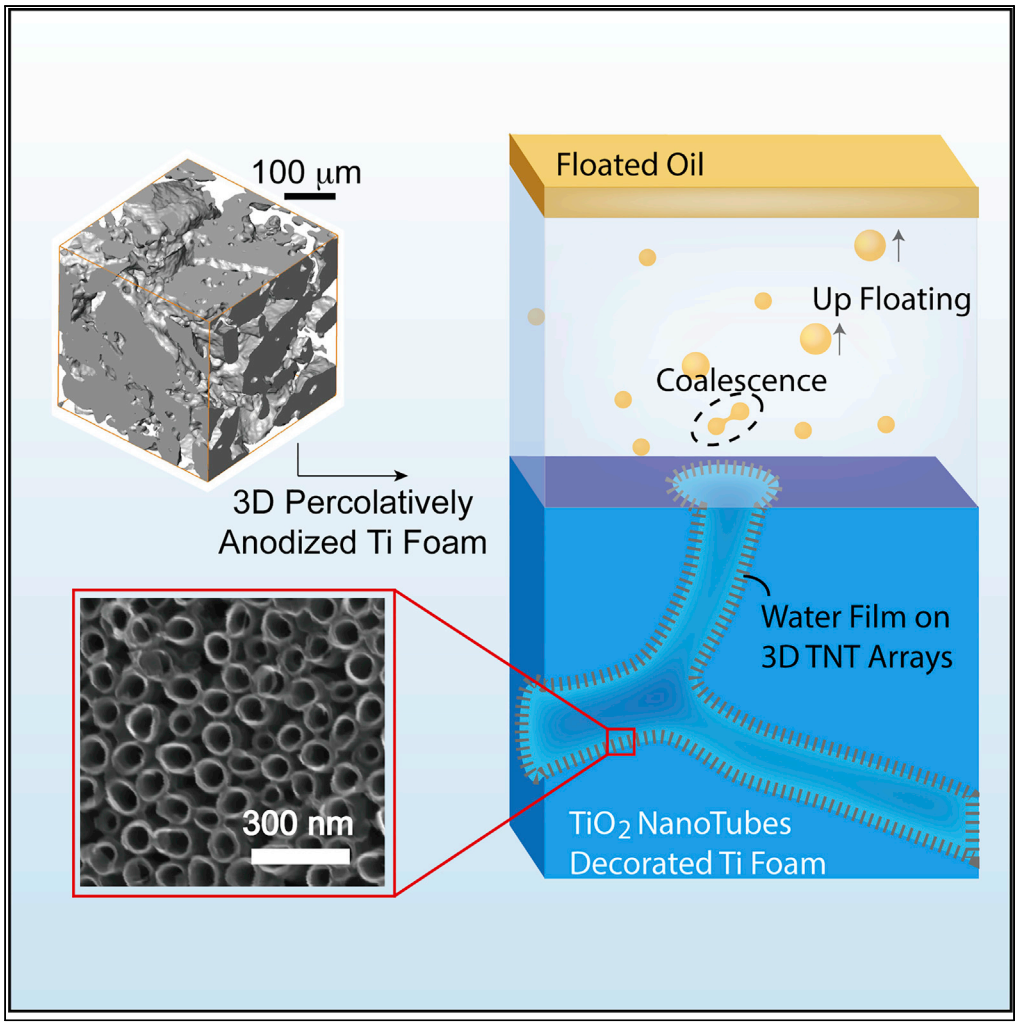

Jian Jin, Xiaoli Zhao, Yong-Hua Du, ..., Chuankun Jia, Zheng Han, Lidong Sun

jack2012ding@gmail.com (C.J.)
vitto.han@gmail.com (Z.H.)
lidong.sun@cqu.edu.cn (L.S.)

HIGHLIGHTS

TiO_2 nanotube arrays percolatively cover entire 3D channels of porous Ti foams

The above-mentioned superhydrophilic foams separate micron-sized oil droplets from water

Separation mechanism of oil-in-water emulsion is studied by the XANES

Jin et al., iScience 6, 289–298
August 31, 2018
https://doi.org/10.1016/j.isci.2018.08.004

iScience

CellPress

Article

Nanostructured Three-Dimensional Percolative Channels for Separation of Oil-in-Water Emulsions

Jian Jin,[1] Xiaoli Zhao,[1] Yong-Hua Du,[2] Mei Ding,[3] Chengjie Xiang,[1] Ning Yan,[4] Chuankun Jia,[3,7,*] Zheng Han,[5,6,*] and Lidong Sun[1,7,8,*]

SUMMARY

Separation of oil/water mixtures has been one of the leading green technologies for applications such as oil recovery and water purification. Conventional methods to separate oil from water are based on phase separation via physical settlement or distillation. However, challenges still remain in the effective extraction of micron-sized oil droplets dispersed in water, in which case gravity fails to work as separating force. Here, we conformably decorate porous titanium (average pore size 30 μm) with superhydrophilic nanotubes. The resulting three-dimensional superhydrophilic micro channels thus provide a driving force for oil-water separation at the nanotube/emulsion interface, enhancing significantly the water infiltration rate. The high efficiency (>99.95%, with oil droplets of average diameter 10 μm) and strong mechanical durability make the structure a reusable oil/water separator. Our findings pave the way for future applications of oil-in-water emulsion separation, which can be readily scaled up for massive demulsification.

INTRODUCTION

Separation of oil from water has been an issue that has developed along with the development of modern technology (Li et al., 2013; Zhou et al., 2018). For example, petroleum manufacturing process has aroused environmental concerns such as oil waste and water pollution (Vlasopoulos et al., 2006). Recent advancement of green technologies has also boosted the need of recovery of oil from water for domestic uses such as kitchen waste recycling (Tuteja et al., 2007; Shimizu and Tanaka, 2017). It is known that by utilizing gravity (Dong et al., 2014), centrifugal force (Krebs et al., 2012), electrochemical means (Ristenpart et al., 2009), or adsorption (Ge et al., 2017), oil/water mixtures can be separated in a macro scale.

However, those conventional methods often fail to work when it comes down to the micro scale, which is most often the case in practical applications (Zeng et al., 2017). To mitigate this, treatments such as chemical agents are often applied in demulsification technology (Jiang et al., 2017). To achieve high-efficiency separation of micron-sized oil droplets in water (i.e., oil-water emulsion), major challenges remain in the high porosity and superhydrophilic surface as concomitants of the material itself. Recently, emerging designs of oil-water emulsion filters, such as organic membranes (Luo and Liu, 2017) and surface-functionalized metal meshes (Zhou et al., 2017a), have become popular in the field of oil/water separation research. Nano-arrays mimicking cacti surface are also reported to be candidates for the effective collection of micron-sized oil droplets from water (Ju et al., 2012). Nevertheless, they either suffer from poor mechanical durability or from an impotent filtering efficiency. To date, a single reusable demulsificator that combines the merits of mechanical durability, high efficiency, and high throughput has been missing.

Among the reported demulsificators, self-organized anodic TiO_2 nanotubes (TNTs) vertically grown on non-planar titanium substrates have attracted tremendous interest because of the superb water wettability (Balaur et al., 2005; Xiang et al., 2017). For example, TNT-covered titanium meshes, wires, and tubes have been used not only in oil/water separation (Sun et al., 2014; Liao et al., 2012) but also in fields such as organic matter degradation (Liao et al., 2012), flexible solar cells (Wen et al., 2016), and Li-ion battery systems (Zhang et al., 2014). The growth mechanism of vertical TiO_2 nanotube arrays (TNTAs) on titanium foams is yet elusive. The reported oil/water separation methods based on TNTAs are mostly limited to the outer surface modification on top of the titanium foams (Li et al., 2015c) and only with low porosity

[1]State Key Laboratory of Mechanical Transmission, School of Materials Science and Engineering, Chongqing University, Chongqing 400044, China

[2]Institute of Chemical and Engineering Sciences, A*STAR, 1 Pesek Road, Jurong Island, Singapore 627833, Singapore

[3]College of Materials Science and Engineering, Changsha University of Science & Technology, Changsha 410114, China

[4]State Key Laboratory of Rolling and Automation, Northeastern University, Shenyang 110819, China

[5]Shenyang National Laboratory for Materials Science, Institute of Metal Research, Chinese Academy of Sciences, Shenyang 110016, China

[6]School of Material Science and Engineering, University of Science and Technology of China, Anhui 230026, China

[7]Key Laboratory of Advanced Energy Materials Chemistry (Ministry of Education), Nankai University, Tianjin 300071, China

[8]Lead Contact

*Correspondence: jack2012ding@gmail.com (C.J.), vitto.han@gmail.com (Z.H.), lidong.sun@cqu.edu.cn (L.S.)

https://doi.org/10.1016/j.isci.2018.08.004

because of the poor oxidation kinetics condition in the micro-pores (Atencia and Beebe, 2005; Wei et al., 2000).

In this work, we show that by developing a three-dimensional (3D) percolative anodization technique, high-porosity titanium framework with thickness reaching a few millimeters can be conformably decorated with superhydrophilic TNT vertical arrays. These 3D percolative superhydrophilic micro channels can serve as "highways" for water but prevent the transport of oil droplets (average size 10 μm, see Supplemental Information). It thus leads to a low-cost reusable oil/water separator with ultrahigh efficiency (>99.95%) and strong mechanical durability.

RESULTS

Fabrication of 3D Percolative Superhydrophilic/Superhydrophobic Micro Channels

Anodization is a commonly used method to produce vertically aligned titania nanotube arrays on Ti surface, which can further tailor the wettability of Ti into a superhydrophilic state (Xiang et al., 2017). Here, to achieve high efficiency, as well as to maintain the mechanical strength of the demulsificator, we chose Ti foam with high porosity and a total thickness of 3–5 mm. As confirmed by 3D micro-computed tomography (CT) in Figure 1A, pore sizes in the foam matrix are of the order of 20–30 μm. The original Ti foams exhibit metallic luster and flat micro-morphology upon a closer look at the surface of the micron-sized pores (Figures 1B–1D).

Open-ended TNTAs are then formed on the titanium foam by anodization in ethylene glycol solution (see Methods). Figure S1C shows the cross-sectional morphologies of the Ti foam with TNTAs grown at 40 V for 40 min in electrolytes with different water contents. Field emission scanning electron microscopic characterization indicates that the nanotubes initiate at the superficial regions (noted as zone A, see Figure S1B) of the Ti foam.

However, rather than nanotubes, titanium oxide films were grown at the inner region (noted as zone B) mostly due to the poor ion diffusion condition in the micro-pores. This outer surface growth of TNTAs on titanium foams was reported previously and has hindered its application in oil/water separation due to poor efficiency (Li et al., 2015c). We have tested different parameters in the anodization process (Supplemental Information), and an optimized anodization duration of 3 hr was used in the electrolyte (n = 4) to synthesize the 3D percolative superhydrophilic TNTAs that conformably cover the high-porosity titanium framework with total thickness reaching a few millimeters. As shown in Figure 1E, after the 3D percolative anodization, the Ti foam with TNTAs presents a dark color (See also Figure S2). The scanning electron micrographic morphologies in Figures 1F and 1G show that the vertically aligned TNTs are open-ended and that the nanotube diameter is distinctly smaller at the top than the bottom, which is assigned to a longer etching duration at the top in the electrolyte and also to the curved channels (see Figure S3).

After a thorough 3D percolative anodization process, we found that both the outer surface (zone A) and inner regions (zone B) can be fully and conformably decorated with vertical TNTAs, as illustrated in Figure 1H. It is noted that, for 3-hr anodization, the average lengths of the nanotubes in zone A are saturated at about 1.8 μm, whereas those in zone B are 0.95 μm, which can linearly increase with longer processing time due to the lagged balance time (see Figure S1E). In addition, the superhydrophilic-to-superhydrophobic transition can be achieved with a chemical modification by *n*-hexane (99%, Adamas) containing 0.5 vol% trichloro (1H,1H,2H,2H-perfluorooctyl) silane (TPFS) on the 3D TNTAs. As will be discussed in the coming sections, for the hydrophilic foam, water infiltration rate reached 173 $\mu L \cdot s^{-1}$, which is 5 orders of magnitudes higher than the original foam.

Surface Wettability Characteristics of Ti Foams with Different Surface Functionalization

In the following, we mainly focus on 5 different types of Ti foams, i.e., the original (without nanotubes, Type I), the as-prepared 3D percolative anodized amorphous TNTAs-decorated Ti foam (superhydrophilic nanotubes, Type II), the annealed 3D percolative anodized TNTAs-decorated Ti foam (superhydrophilic nanotubes, Type III), the TPFS-treated amorphous TNTAs-decorated Ti foam (superhydrophobic nanotubes, Type IV), and the TPFS-treated annealed TNTAs-decorated Ti foam (superhydrophobic nanotubes, Type V). As shown in Figure S4, drop impact tests were performed to verify the surface wettability characteristics of each type of foam. The visual test process of types II and III is recorded in Video S1. The results indicate that, for the original titanium foam, the water droplet adhered to the foam and presented a viscous hydrophobic state. However, the water droplet instantly spread on the Type II/III foams, due to the

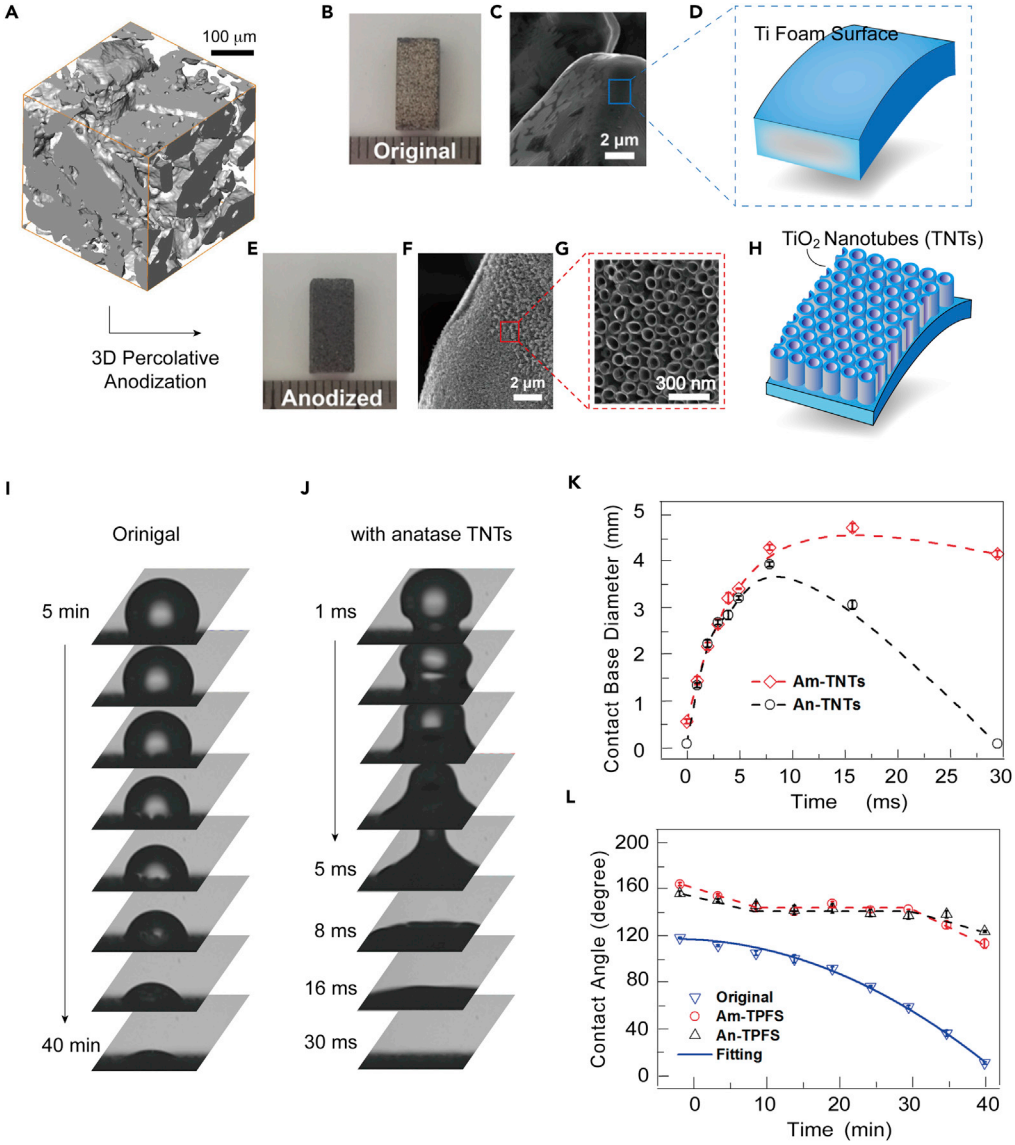

Figure 1. Morphology and Wetting Properties of 3D-TNTAs

(A) 3D topological morphology of the pristine Ti foam, obtained by the 3D micro-CT technique.

(B–J) Photograph (B, E) and scanning electron micrographs (C, F, and G) of an original Ti foam (B, C) and that conformably coated with TNTs (E–G). Corresponding illustrations are given in (D) and (H), respectively. Time sequence of video frames showing the evolution of water droplet on original (I) and anatase-TNT-coated (J) foams.

(K and L) Contact base diameter (K) and contact angle (L) as a function of time for superhydrophilic (amorphous nanotubes, Am-TNTs; anatase nanotubes, An-TNTs) and superhydrophobic (amorphous nanotubes with TPFS treatment, Am-TPFS; anatase nanotubes with TPFS treatment, An-TPFS) foams. Each of the data point in (K) and (L) was based on at least three samples.

See also Figures S1–S7, and S10, and Table S1.

composite 3D structure of micro-pores and the superhydrophilic TNTAs. A superhydrophobic behavior was observed on the Type IV/V foams, as the droplet rolls freely on the foam, similar to the behavior of water droplet on a lotus leaf.

The evaluation of sessile water droplet on foams with different wettability is shown in Figures 1I, 1J, and S5. The water droplet infiltrated after about 40 min on the original foam (Type I). For the Type I foam, there was an evaporation effect during the capillary absorption of water droplet. The evaporation rate can be estimated based on the tests on superhydrophobic foams (Types IV and V); under such conditions, evaporation

dominates the mass loss with negligible infiltration. The droplet volume was decreased from 5 to 2.1 μL in 40 min (see Figure S5), resulting in an evaporation rate of about 1.2×10^{-3} μL•s^{-1}. For the original foam, the same evaporation rate was assumed and the droplet volume was reduced to 1.7 μL in 20 min, which was assigned to the combined results of evaporation and infiltration. Accordingly, an infiltration rate of about 1.6×10^{-3} μL•s^{-1} was obtained for the original foams.

The evaporation effect can be ignored for Type II and III foams, because the lifetime of a droplet is within tens of milliseconds. When a sessile drop is contacted to Type II/III foams, a strong deformation of the droplet was led by the interaction between the collision and the capture actions from the foam, which is presented as a regular pattern. Before being captured, the droplet was spherical, but the solid-liquid interface rapidly expanded in a few milliseconds after contact. As opposed to the Type I foam, the infiltration time of water droplet increased by more than 10,000 times on the Type II/III foams, with the water droplet disappearing within about 30 ms, as shown in Figure 1J.

It is noticed that, in Figure 1J, at the first contact with the Type III foam, part of the water droplet tended to jump into the air due to inertia, but it was pulled down because of the cohesive force, giving rise to the transformation from a ball to a hat shape after 3 ms. The hat-like droplet gradually collapsed and finally disappeared completely. The droplet permeated into the foam under capillary effect, which caused horizontal and vertical imbibitions. As shown in Figure 1K, the horizontal imbibition is conducive to the expansion of the base diameter because of its lubrication effect, whereas the vertical imbibition contributes to the shrinking of the diameter. Therefore, the base diameter then shrunk when the vertical imbibition was dominant. The dynamic evaluation is recorded in Video S1. As only capillary effect was taken into account, the infiltration time of Type III foam is about 4 times greater than that of Type II foam (30 versus 130 ms). The greater rate is caused by better vertical imbibition action in the micro-pores, resulting from the improved hydrophilicity of the TNTs upon crystallization via thermal annealing. More capillary tests can be found in Figures S6 and S7. The average infiltration rate for the micro-droplet is estimated to 173 μL•s^{-1} for the Type III foam, which is about 5 orders enhancement when compared with the original foam (173 versus 1.6×10^{-3} μL•s^{-1}).

Figure 1L shows the static contact angle evolution of water droplet on the Type I, Type IV, and Type V foams. The contact angle decreases exponentially as the exposure time for the original foam (Type I) and the relation between them can be expressed by the fitting formula (Motulsky and Ransnas, 1987):

$$\theta = 120.24–0.0097t– 0.059t^2 \qquad \text{(Equation 1)}$$

where θ and t are the contact angle (degree) and time (minute), respectively. It can be calculated from the formula that the hydrophobic-hydrophilic transition occurred at about 22 min. Also, the rate of reduction of contact angle linearly increases with time, resulting from the increased pinning effect caused by capillary penetration. For the TPFS-treated superhydrophobic foams with amorphous and annealed TNTAs (Types IV and V), contact angle evolution curves are almost identical to each other and can be divided into 3 stages. Their initial contact angles both decrease linearly with time, and these decreasing trends were terminated after around 10 min and then leveled off in the second stage. When the exposure time reached 30 min, the contact angle dropped again quickly. Based on Cassie-Baxter's model (Cassie and Baxter, 1944), the liquid cannot infiltrate into the micro-pores and pits on solid surfaces and the air is trapped under the droplet for superhydrophobic surfaces. The evaporation effect is the single factor affecting the contact angle for the Am- (amorphous) and An- (anatase) TPFS (i.e., Types IV and V) foams. Therefore, as shown in Figure 1L, the initial contact angles were both more than 150° and first deceased to the receding angle θ_r because of a hysteresis effect that originated from the pinning action on the porous surface. Thereafter, the contact angle remained constant because of the reduced pinning resistance. However, the contact angle dropped again after 30 min, which may be caused by the collapsed air pockets with the liquid permeating into the foams. Therefore, the effective time was 30 min for resistance to imbibition for a micro-droplet. Our results therefore successfully demonstrated the superhydrophilic-to-superhydrophobic transition by a chemical modification with TPFS on the Ti foam with 3D percolative TNTAs.

3D Percolative TiO_2 Nanotube Arrays-Decorated Ti Foam with Millimeter Thickness for Oil-in-Water Emulsion Separation

To test the oil/water separation capability of the 3D TNTAs-decorated Ti foams, 4 kinds of oil-in-water emulsions (hexane, xylene, octane, and chlorobenzene) were prepared. A vertical deployment of

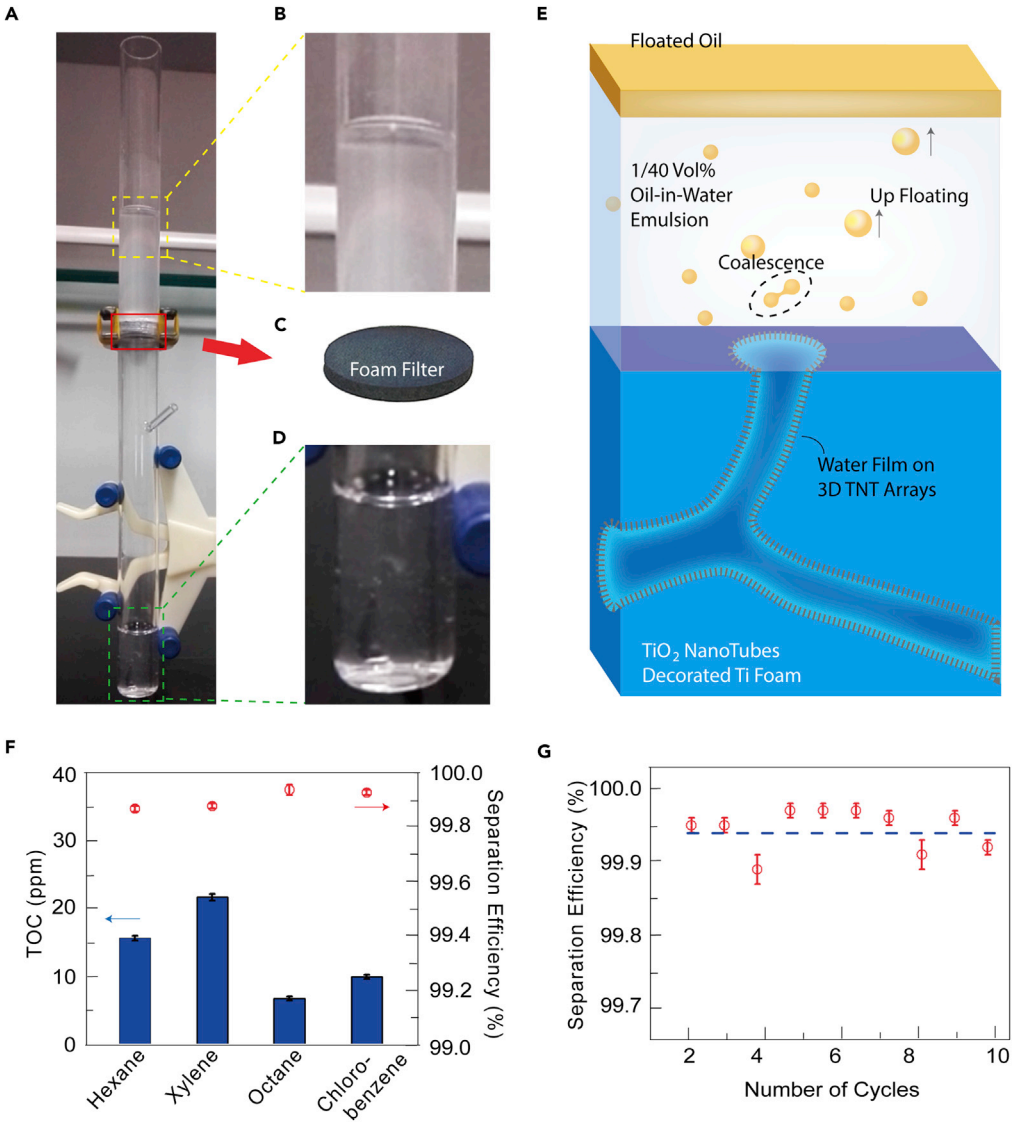

Figure 2. Demonstration of Oil-in-Water Emulsion Separation by 3D-TNTs

(A–D) (A) Experimental setup of vertical deployment, where local magnifications are given in (B–D).

(E) Illustration showing the separation mechanism.

(F) The amount of total organic carbon in filtrates and the corresponding separation efficiency using different emulsions.

(G) Recycling tests of the superhydrophilic foam (Type III) employing octane-in-water emulsion. Each of the data point in (F) and (G) was based on at least three samples.

See also Figures S6, S8, and S9.

oil-in-water emulsion separation device is shown in Figure 2A. The upper quartz tube is the feeding container with emulsion, and the lower one is installed to collect the filtrated water, as shown in Figures 2B and 2D. The 3D TNTAs-decorated foam (Type III) with a thickness of 3 mm (Figure 2C) was fixed between 2 tubes for emulsion separation. The separation process is driven by gravity and is recorded in Video S2. A schematic of the separation mechanism of oil-in-water emulsion is illustrated in Figure 2E. Finite oil droplets freely disperse in the emulsion, and their diameter ranges from several microns to tens of microns (Figure S8). When the foam contacts the emulsion, the intrusion pressure of water is decreased ($\Delta p_1<0$), resulting from the superhydrophilic TNTAs, and the foam is completely wetted in the timescale of milliseconds under 3D capillary force (see Figure S9). Those oil droplets moving toward the foam under the downward permeation flow cannot directly pass through the foam because the intrusion pressure of oil is opposite to the flow direction ($\Delta p_2>0$, Figure S9). Therefore, the micron-sized oil droplets gathering near the foam

surface tend to coalesce into larger sized droplets (Figure 2E), due to the improved oil droplet density at the surface. The coalesced oil droplets are then released from the surface and float up because of the increased buoyancy. Finally, the droplets float on top of the water and a free oil layer appears, as observed in the process (Figure 2B).

To emphasize the importance of the 3D percolative anodization of TNTAs, we compare the oil/water separation performance between the Type III foam and the original Ti foam, as shown in Videos S2 and S3, respectively. In addition, it is essential to also compare with those only anodized at the surface (zone A), while the core of the foam are not coated conformably with TNTs, as seen in many conventional anodized Ti foams (Li et al., 2015c).

To demonstrate it more precisely, only one surface in zone A was coated with nanotubes (referred to as single-sided superhydrophilic foam). The visual performance of oil-in-water emulsion separation using the single-sided foam is shown in Video S4, with its water absorption test given in Figure S7 and evolution of water droplet in Figure S10. Type III foam shows the best performance in terms of separation speed and efficiency, wherein the white emulsion turned transparent after separation from the TNTAs-decorated Ti foam (Video S2). For the original and the superficially anodized foams, the filtrate is still turbid with a lot of oil droplets in water, or frequently the foams are even clogged by the emulsion.

To quantitatively study the efficiency of oil-in-water emulsion separation, the content of total organic carbon (TOC) in the filtrated water from 4 kinds of emulsions was measured. As shown in Figure 2F, for all emulsions, the TOC content is lower than 25 ppm, and the TOC content is as low as 7.5 ppm for octane-in-water emulsion. The corresponding separation efficiencies are stabilized around 99.9% for different emulsions, and, specially, an efficiency of 99.95% is obtained for octane-in-water emulsion. The recycled separation was carried out for octane-in-water emulsion to evaluate the separation stability of the TNTAs-decorated foam. As shown in Figure 2G the separation efficiency maintained after 10 cycles, which illustrates that the TNTAs-decorated Ti foam has a good cycling stability for emulsion separation.

DISCUSSION

Demonstration of a Self-Driven Siphon-like Demulsificator

As a proof of principle for realizing self-driven high-speed demulsificator using the 3-mm 3D TNTAs-decorated Ti foam, we used a simple siphon setup to separate octane-in-water emulsion with droplet size of the order of 10–20 μm. As shown in Figures 3A and 3B and Figure S11 oil-in-water emulsion can indeed be effectively separated by the self-driven Siphon effect (visual tests of the Siphon device as well as capillary forces can be seen in Videos S5, S6, and S7). In our demonstration, a Type III foam having cross section of about 3.1 cm^2 was used in the link between 2 containers, which leads to a filtration rate of about 120 $L \cdot m^{-2} \cdot h^{-1}$ based on the slope in the linear section (Figure 3C).

Furthermore, the compressive stress-strain curves of the original and TNTAs-decorated Ti foams are shown in Figure S12. For the 3D percolative TNTAs-decorated Ti foam, the compressive resistance is in line with that of the original foams. Here, the yield strength of titanium foam reaches 75 MPa, which is much higher than that of other inorganic materials used in the field of oil/water separation (Xu et al., 2012; Biswas et al., 2016). As a comparison, the commonly used organic oil/water separation membrane polyvinylidene fluoride has a very poor compressive property (Cui et al., 2014), whereas the inorganic materials perform relatively better.

It therefore indicates the feasibility of massive demulsification in an industrial scale, namely, by enlarging the area of the foam filter, using the Siphon effect, one can achieve high-speed and high-efficiency oil-in-water emulsions with ultrafine oil droplets (diameter of ~10 μm), while keeping its mechanical strength and presenting outstanding cycling-stability.

Characterizations of the Foams Using X-Ray Absorption Near-Edge Spectroscopy

To understand the mechanism of water wettability to the TNTAs on Ti foam, *in situ* X-ray absorption near-edge spectroscopy (XANES) (see Figure S13 for the experimental setup) was used to probe the bonding between TNTs and different liquids. As shown in Figures 3D and 3E, the absorption profile of Ti K-edge (the first derivative of XANES) is illustrated along with Gaussian fits of each peak in the energy window of Ti K-edge. The absorption profile of TNTs shows negligible changes when immerged in octane. This

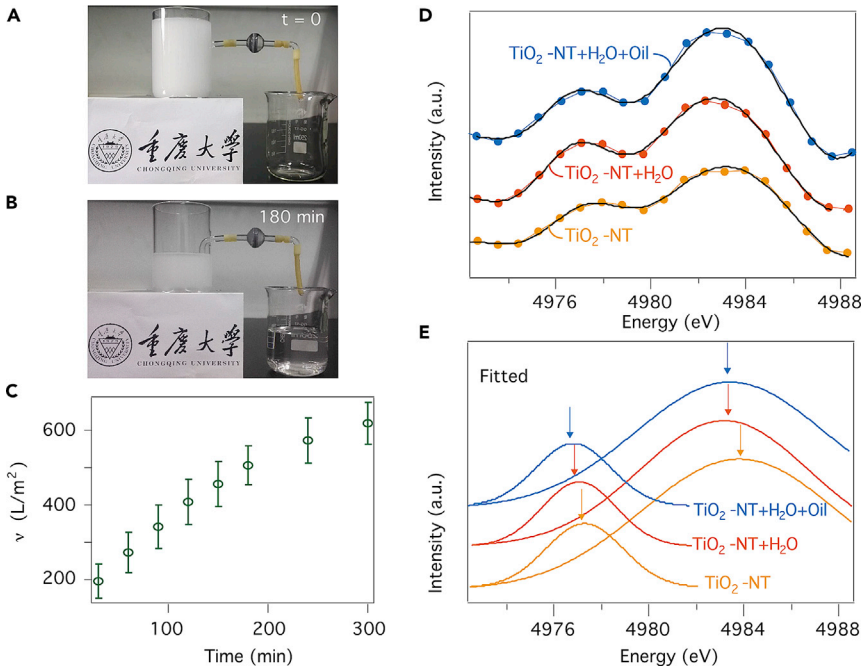

Figure 3. Siphon-like Demulsificator and the XANES Analysis

(A and B) An oil filter for octane-in-water emulsion in the configuration of a siphon.

(C) Filtrate volume per unit medium area (ν) of the prototype siphon filter as a function of time. Each of the data point was based on at least three independent measurements.

(D and E) The first derivative of XANES of Ti K-edge for TiO_2 nanotubes (TiO_2-NT, yellow) and that immerged in water (TiO_2-NT + H_2O, orange) and octane-in-water emulsion (TiO_2-NT + H_2O + oil, blue).

See also Figures S11–S13.

suggests a weak interaction between TiO_2 and octane, as no functional groups are present in the molecule. In contrast, the profile exhibits substantial red shift upon immerging in water. This is attributed to the bonding between the Ti^{4+} ions at TiO_2 surface and the OH^- groups in water, lowering the chemical states of Ti^{4+} ions (Henderson, 1996; Fujishima and Honda, 1972).

Figure 3E displays a similar red shift once the nanotubes are in contact with the octane-in-water emulsion. It indicates that the water molecules in the emulsion have a high priority of bonding with the nanotubes, in light of their rapid infiltration time (30 versus 150 ms) and high volume ratio (40: 1) when compared with octane. As such, the following mechanism dominates in the process of oil/water separation. The moment the emulsion meets the superhydrophilic foam, a water film is developed immediately in the micro channels via OH^- groups. This expels most of the oil droplets at the estuary of the channels, in view of the immiscibility between oil and water. Even though a few droplets of small size are involved, it is difficult for them to pass through the 3D channels of irregular feature, thus being driven out eventually.

Comparison of the State-of-the-Art Oil/Water Separators

To further illustrate the separation performance, the emulsion separation efficiency of the 3D percolative TNTAs-decorated Ti foam was compared with that in other studies, as shown in Figure 4. The abscissa is a dimensionless value, which is the ratio of the thickness to the average pore size for porous separation materials. This ratio, however, represents highly the essence of the desired filter, as for oil-in-water emulsion separation, the increase in the thickness is usually beneficial to enhance the separation efficiency due to the longer micro channel, whereas the smaller pore size is expected because the screening effect is stronger for oil droplet.

A reasonable combination of the thickness and pore size is required, because the measures can reduce the flow and channel clogging problems may occur. The result shows that the 3D percolative TNTAs-decorated Ti foam have an outstanding oil/water separation performance whether in organic or inorganic oil/water

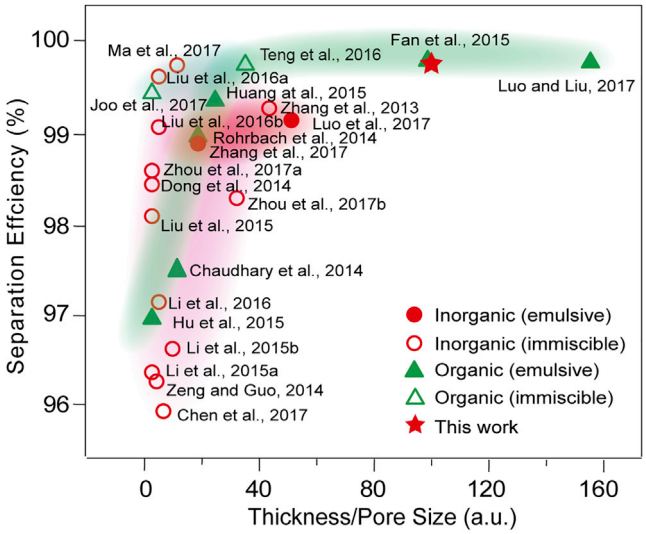

Figure 4. Statistics on Various Demulsificators

The diagram compares the oil-in-water emulsion separation properties of the current work with that of other reports. (Chaudhary et al., 2014; Chen et al., 2017; Fan et al., 2015; Hu et al., 2015; Huang et al., 2015; Joo et al., 2017; Li et al., 2015a, 2015b; Li et al., 2016; Liu et al., 2016a; Liu et al., 2016b; Liu et al., 2015; Luo et al., 2017; Ma et al., 2017; Rohrbach et al., 2014; Teng et al., 2016; Zeng and Guo, 2014; Zhang et al., 2013; Zhang et al., 2017; Zhou et al., 2017b).

separation material system. Especially, the separation efficiency is also dazzling among the materials for oil-in-water emulsion separation.

Conclusion

We have demonstrated a 3D percolative anodization technique with which high-porosity titanium framework with thickness reaching a few millimeters can be conformably decorated with superhydrophilic TNT vertical arrays. These 3D percolative superhydrophilic micro channels can serve as a "highway" for water but prevent the transport of oil molecules. This results in a reusable oil/water separator that filters oil droplets of average diameter 10 μm, with >99.95% efficiency and strong mechanical durability. Moreover, those 3D percolative micro channels can be further turned into superhydrophobic by TPFS treatment, which may expand the application of TNTAs-decorated Ti foam into another limit of the water-in-oil emulsion. Our studies show that nanostructure-modified percolative metal frameworks hold great promise for future demulsification technology.

METHODS

All methods can be found in the accompanying Transparent Methods supplemental file.

SUPPLEMENTAL INFORMATION

Supplemental Information includes Transparent Methods, 13 figures, 1 table, and 7 videos and can be found with this article online at https://doi.org/10.1016/j.isci.2018.08.004.

ACKNOWLEDGMENTS

This work is supported by the National Natural Science Foundation of China (NSFC, Nos. 51871037, 51501024, 11504385, and 51627801), the Chongqing Research Program of Basic Research and Frontier Technology (No. cstc2015jcyjA90004), and the Fundamental Research Funds for the Central Universities (No.2018CDQYCL0027). L.S. and C.J. are grateful for support of the 111 project (B12015) at the Key Laboratory of Advanced Energy Materials Chemistry (Ministry of Education), Nankai University.

AUTHOR CONTRIBUTIONS

L.S., Z.H., and C.J. conceived the idea, designed the experiments, analyzed the data, and wrote the paper. J.J. carried out the experiments, analyzed the data, and wrote the initial draft. X.Z. and C.X. prepared the

samples for XANES measurements. Y-H.D. conducted the XANES measurements and analyzed the data. M.D. and N.Y. participated in the discussion of the results. All authors commented on the manuscript.

DECLARATION OF INTERESTS

L.S., J.J., Z.H., M.D., and C.J. have a Chinese patent application (application no. 201711473117.1) pertinent to this study. The authors declare no financial interest.

Received: May 23, 2018
Revised: July 7, 2018
Accepted: August 7, 2018
Published: August 31, 2018

REFERENCES

Atencia, J., and Beebe, D.J. (2005). Controlled microfluidic interfaces. Nature *437*, 648–655.

Balaur, E., Macak, J.M., Tsuchiya, H., and Schmuki, P. (2005). Wetting behaviour of layers of TiO_2 nanotubes with different diameters. J. Mater. Chem. *15*, 4488–4491.

Biswas, P., Ramavath, P., Nair, C.M., Suresh, M.B., Ravi, N., and Johnson, R. (2016). Quasi-static compression behavior of nickel oxide, nickel oxide: zirconia, nickel: zirconia and nickel foams. Ceram. Int. *42*, 10572–10578.

Cassie, A.B.D., and Baxter, S. (1944). Wettability of porous surfaces. Trans. Faraday Soc. *40*, 546–551.

Chaudhary, J.P., Nataraj, S.K., Gogda, A., and Meena, R. (2014). Bio-based superhydrophilic foam membranes for sustainable oil-water separation. Green Chem. *16*, 4552–4558.

Chen, X., He, Y., Fan, Y., Yang, Q., Zeng, G., and Shi, H. (2017). Facile fabrication of a robust superwetting three-dimensional (3D) nickel foam for oil/water separation. J. Mater. Sci. *52*, 2169–2179.

Cui, Z., Drioli, E., and Lee, Y.M. (2014). Recent progress in fluoropolymers for membranes. Prog. Polym. Sci. *39*, 164–198.

Dong, Y., Li, J., Shi, L., Wang, X., Guo, Z., and Liu, W. (2014). Underwater superoleophobic graphene oxide coated meshes for the separation of oil and water. Chem. Commun. (Camb.) *50*, 5586–5589.

Fan, J.B., Song, Y., Wang, S., Meng, J., Yang, G., Guo, X., Feng, L., and Jiang, L. (2015). Directly coating hydrogel on filter paper for effective oil-water separation in highly acidic, alkaline, and salty environment. Adv. Funct. Mater. *25*, 5368–5375.

Fujishima, A., and Honda, K. (1972). Electrochemical photolysis of water at a semiconductor electrode. Nature *238*, 37–38.

Ge, J., Shi, L.A., Wang, Y.C., Zhao, H.Y., Yao, H.B., Zhu, Y.B., Zhang, Y., Zhu, H.W., Wu, H.A., and Yu, S.H. (2017). Joule-heated graphene-wrapped sponge enables fast clean-up of viscous crude-oil spill. Nat. Nanotechnol. *12*, 434–440.

Henderson, M.A. (1996). Structural sensitivity in the dissociation of water on TiO_2 single-crystal surfaces. Langmuir *12*, 5093–5098.

Hu, L., Gao, S., Zhu, Y., Zhang, F., Jiang, L., and Jin, J. (2015). An ultrathin bilayer membrane with asymmetric wettability for pressure responsive oil/water emulsion separation. J. Mater. Chem. A *3*, 23477–23482.

Huang, T., Zhang, L., Chen, H., and Gao, C. (2015). Sol-gel fabrication of a non-laminated graphene oxide membrane for oil/water separation. J. Mater. Chem. A *3*, 19517–19524.

Jiang, G., Fu, W., Wang, Y., Liu, X., Zhang, Y., Dong, F., Zhang, Z., Zhang, X., Huang, Y., Zhang, S., et al. (2017). Calcium sulfate hemihydrate nanowires: one robust material in separation of water from water-in-oil emulsion. Environ. Sci. Technol. *51*, 10519–10525.

Joo, M., Shin, J., Kim, J., You, J.B., Yoo, Y., Kwak, M.J., Oh, M.S., and Im, S.G. (2017). One-step synthesis of cross-inked ionic polymer thin films in vapor phase and its application to an oil/water separation membrane. J. Am. Chem. Soc. *139*, 2329–2337.

Ju, J., Bai, H., Zheng, Y., Zhao, T., Fang, R., and Jiang, L. (2012). A multi-structural and multi-functional integrated fog collection system in cactus. Nat. Commun. *3*, 1247.

Krebs, T., Schroen, C.G.P.H., and Boom, R.M. (2012). Separation kinetics of an oil-in-water emulsion under enhanced gravity. Chem. Eng. Sci. *71*, 118–125.

Li, J., Yan, L., Li, H., Li, W., Zha, F., and Lei, Z. (2015a). Underwater superoleophobic palygorskite coated meshes for efficient oil/water separation. J. Mater. Chem. A *3*, 14696–14702.

Li, J., Yan, L., Li, W., Li, J., Zha, F., and Lei, Z. (2015b). Superhydrophilic-underwater superoleophobic ZnO-based coated mesh for highly efficient oil and water separation. Mater. Lett. *153*, 62–65.

Li, L., Liu, Z., Zhang, Q., Meng, C., Zhang, T., and Zhai, J. (2015c). Underwater superoleophobic porous membrane based on hierarchical TiO_2 nanotubes: multifunctional integration of oil-water separation, flow-through photocatalysis and self-cleaning. J. Mater. Chem. A *3*, 1279–1286.

Li, J., Li, D., Yang, Y., Li, J., Zha, F., and Lei, Z. (2016). A prewetting induced underwater superoleophobic or under oil (super) hydrophobic waste potato residue-coated mesh for selective efficient oil/water separation. Green Chem. *18*, 541–549.

Li, K., Ju, J., Xue, Z.X., Ma, J., Feng, L., Gao, S., and Jiang, L. (2013). Structured cone arrays for continuous and effective collection of micron-sized oil droplets from water. Nat. Commun. *4*, 2276.

Liao, J., Lin, S., Zhang, L., Pan, N.Q., Cao, X., and Li, J. (2012). Photocatalytic degradation of methyl orange using a TiO_2/Ti mesh electrode with 3D nanotube arrays. ACS Appl. Mater. Interfaces *4*, 171–177.

Liu, J., Wang, L., Guo, F., Hou, L., Chen, Y., Liu, J., Wang, N., Zhao, Y., and Jiang, L. (2016a). Opposite and complementary: a superhydrophobic-superhydrophilic integrated system for high-flux, high-efficiency and continuous oil/water separation. J. Mater. Chem. A *4*, 4365–4370.

Liu, L., Chen, C., Yang, S., Xie, H., Gong, M.G., and Xu, X. (2016b). Fabrication of superhydrophilic-underwater superoleophobic inorganic anti-corrosive membranes for high-efficiency oil/water separation. Phys. Chem. Chem. Phys. *18*, 1317–1325.

Liu, M., Li, J., Shi, L., and Guo, Z. (2015). Stable underwater superoleophobic conductive polymer coated meshes for high-efficiency oil-water separation. RSC Adv. *5*, 33077–33082.

Luo, C., and Liu, Q. (2017). Oxidant-induced high-efficient mussel-inspired modification on PVDF membrane with superhydrophilicity and underwater superoleophobicity characteristics for oil/water separation. ACS Appl. Mater. Interfaces *9*, 8297–8307.

Luo, Z.Y., Lyu, S.S., Wang, Y.Q., and Mo, D.C. (2017). Fluorine-induced superhydrophilic Ti foam with surface nanocavities for effective oil-in-water emulsion separation. Ind. Eng. Chem. Res. *56*, 699–707.

Ma, Q., Cheng, H., Yu, Y., Huang, Y., Lu, Q., Han, S., Chen, J., Wang, R., Fane, A.G., and Zhang, H. (2017). Preparation of superhydrophilic and underwater superoleophobic nanofiber-based meshes from waste glass for multifunctional oil/water separation. Small *13*, 1700391.

Motulsky, H.J., and Ransnas, L.A. (1987). Fitting curves to data using nonlinear regression: a practical and nonmathematical review. FASEB J. *1*, 365–374.

Ristenpart, W.D., Bird, J.C., Belmonte, A., Dollar, F., and Stone, H.A. (2009). Non-coalescence of oppositely charged drops. Nature *461*, 377–380.

Rohrbach, K., Li, Y., Zhu, H., Liu, Z., Dai, J., Andreasen, J., and Hu, L. (2014). A cellulose based hydrophilic, oleophobic hydrated filter for water/oil separation. Chem. Commun. (Camb.) *50*, 13296–13299.

Shimizu, R., and Tanaka, H. (2017). Impact of complex topology of porous media on phase separation of binary mixtures. Sci. Adv. *3*, 9570.

Sun, L., Zhang, S., and Wang, Q. (2014). Conformal growth of anodic nanotubes for dye-sensitized solar cells: part II. nonplanar electrode. J. Nanosci. Nanotechnol. *14*, 2050–2064.

Teng, C., Xie, D., Wang, J., Zhu, Y., and Jiang, L. (2016). A strong, underwater superoleophobic PNIPAM–clay nanocomposite hydrogel. J. Mater. Chem. A *4*, 12884–12888.

Tuteja, A., Choi, W., Ma, M., Mabry, J.M., Mazzella, S.A., Rutledge, G.C., Mckinley, G.H., and Cohen, R.E. (2007). Designing superoleophobic surfaces. Science *318*, 1618–1622.

Vlasopoulos, N., Memon, F.A., Bulter, D., and Murphy, R. (2006). Life cycle assessment of wastewater treatment technologies treating petroleum process waters. Sci. Total Environ. *367*, 58–70.

Wei, Q.-H., Bechinger, C., and Leiderer, P. (2000). Single-file diffusion of colloids in one-dimensional channels. Science *287*, 625–627.

Wen, Z., Yeh, M.H., Guo, H., Wang, J., Zi, Y., Xu, W., Deng, J., Zhu, L., Wang, X., Hu, C., et al. (2016). Self-powered textile for wearable electronics by hybridizing fiber-shaped nanogenerators, solar cells, and supercapacitors. Sci. Adv. *2*, e1600097.

Xiang, C., Sun, L., Wang, Y., Wang, G., Zhao, X., and Zhang, S. (2017). Large-scale, uniform, and superhydrophobic titania nanotubes at the inner surface of 1000 mm long titanium tubes. J. Phys. Chem. C *121*, 15448–15455.

Xu, Z.G., Fu, J.W., Luo, T.J., and Yang, Y.S. (2012). Effects of cell size on quasi-static compressive properties of Mg alloy foams. Mater. Des. *34*, 40–44.

Zeng, J., and Guo, Z. (2014). Superhydrophilic and underwater superoleophobic MFI zeolite-coated film for oil/water separation. Colloids Surf. A *444*, 283–288.

Zeng, X., Qian, L., Yuan, X., Zhou, C., Li, Z., Cheng, J., Xu, S., Wang, S., Pi, P., and Wen, X. (2017). Inspired by Stenocara beetles: from water collection to high-efficiency water-in-oil emulsion separation. ACS Nano *11*, 760–769.

Zhang, F., Zhang, W.B., Shi, Z., Wang, D., Jin, J., and Jiang, L. (2013). Nanowire-haired inorganic membranes with superhydrophilicity and underwater ultralow adhesive superoleophobicity for high-efficiency oil/water separation. Adv. Mater. *25*, 4192–4198.

Zhang, Y.Q., Bin Yang, X., Wang, Z.X., Long, J., and Shao, L. (2017). Designing multifunctional 3D magnetic foam for effective insoluble oil separation and rapid selective dye removal for use in wastewater remediation. J. Mater. Chem. A *5*, 7316–7325.

Zhang, Z.J., Zeng, Q.Y., Chou, S.L., Li, X.J., Li, H.J., Ozawa, K., Liu, H.K., and Wang, J.Z. (2014). Tuning three-dimensional TiO_2 nanotube electrode to achieve high utilization of Ti substrate for lithium storage. Electrochim. Acta *133*, 570–577.

Zhou, C., Cheng, J., Hou, K., Zhu, Z., and Zheng, Y. (2017a). Preparation of $CuWO_4$@Cu_2O film on copper mesh by anodization for oil/water separation and aqueous pollutant degradation. Chem. Eng. J. *307*, 803–811.

Zhou, C., Li, Y., Li, H., Zeng, X., Pi, P., Wen, X., Xu, S., and Cheng, J. (2017b). A self-cleaning titanium mesh with underwater superoleophobicity for oil/water separation and aqueous pollutant degradation. Surf. Coat. Technol. *313*, 55–62.

Zhou, C., Feng, J., Cheng, J., Zhang, H., Lin, J., Zeng, X., and Pi, P. (2018). Opposite superwetting nickel meshes for on-demand and continuous oil/water separation. Ind. Eng. Chem. Res. *57*, 1059–1070.

ISCI, Volume *6*

Supplemental Information

Nanostructured Three-Dimensional Percolative Channels for Separation of Oil-in-Water Emulsions

Jian Jin, Xiaoli Zhao, Yong-Hua Du, Mei Ding, Chengjie Xiang, Ning Yan, Chuankun Jia, Zheng Han, and Lidong Sun

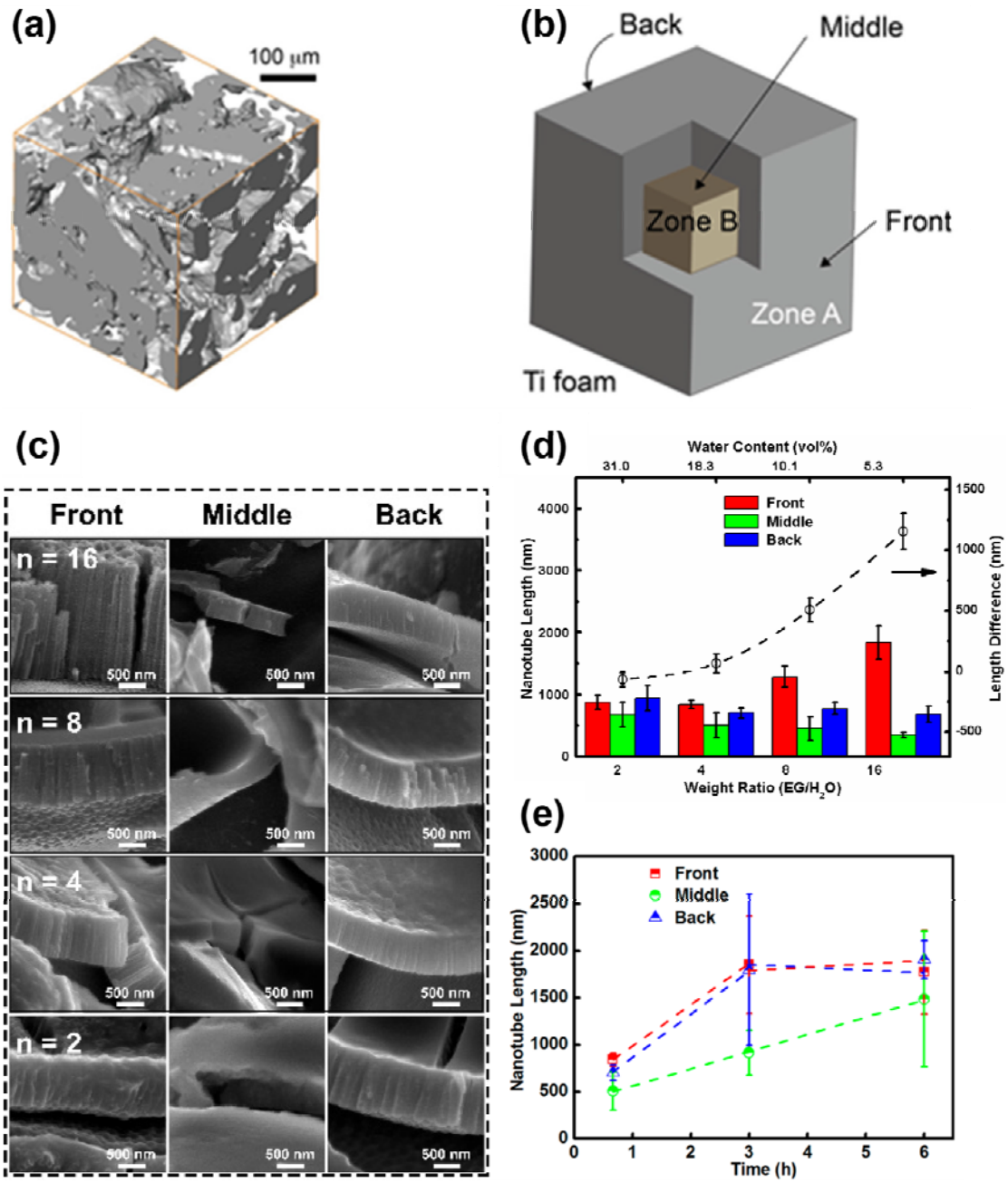

Figure S1. Structure optimization of TNTAs on Ti foams, related to Figure 1. (a) Micro-CT image of the Ti foam; (b) Schematic of outer and inner regimes, denoted as Zone A and Zone B, as the inner Zone B is more difficult to be fully covered with TiO_2 nanotubes during the anodization process; (c) SEM images of the three representative regions (Front: the regions close to the Ti foam surface that faces the cathode, Back: the regions close to the other surface, Middle: the regions in between, as illustrated in (b)) in Ti foams of 3 mm in thickness, which were obtained using electrolytes of different weight ratios (n=2, 4, 8, 16) of ethylene glycol (EG) to water; (d) Corresponding nanotube length (left) and length difference between the Front and Back (right) under the conditions in (c); (e) Time dependence of tube length at different positions when n=4 for different durations. Each of the tube length is based on 3–5 samples and at least 10 FESEM images for each sample.

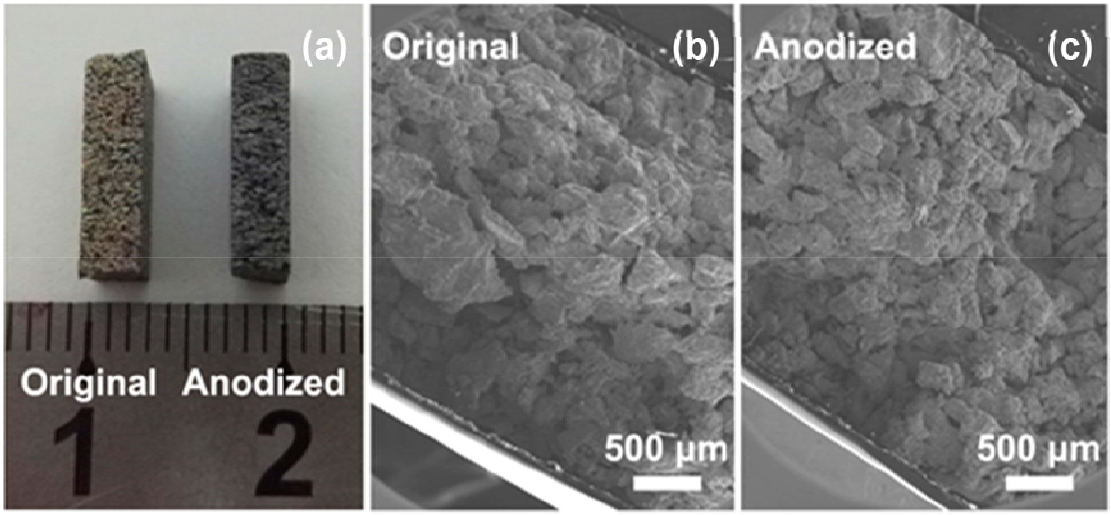

Figure S2. Morphologies of original and anodized Ti foams, related to Figure 1. (a) Comparison of optical morphology of original and anodized Ti foam used in this work. Their low-magnification SEM images are given in (b) and (c), respectively.

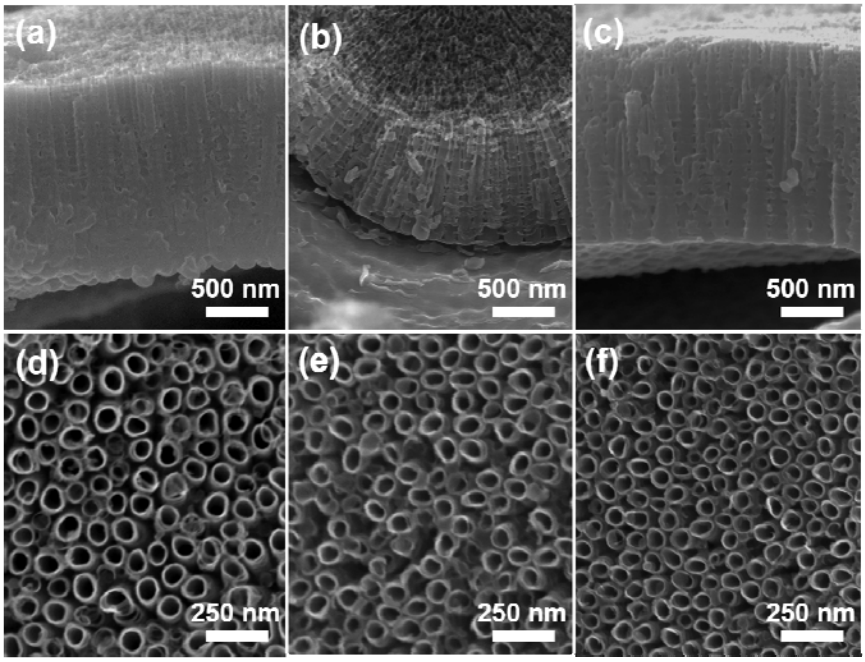

Figure S3. Features of TNTAs used for oil-water separation, related to Figure 1. Cross-sectional (a–c) and surface (d–f) FESEM images of the TiO_2 nanotube arrays prepared in ethylene glycol containing 18.3 vol% water (weight ratio n=4) and 0.3 wt% NH_4F at 40 V and 22 °C for 3 h, with the distance between anode and cathode being kept at 12 mm. Such conditions were employed to fabricate conformal nanotube coatings inside Ti foams for subsequent oil-water separation application. The panels from left to right are nanotube coatings at the front (a, d), middle (b, e), and back (c, f), respectively.

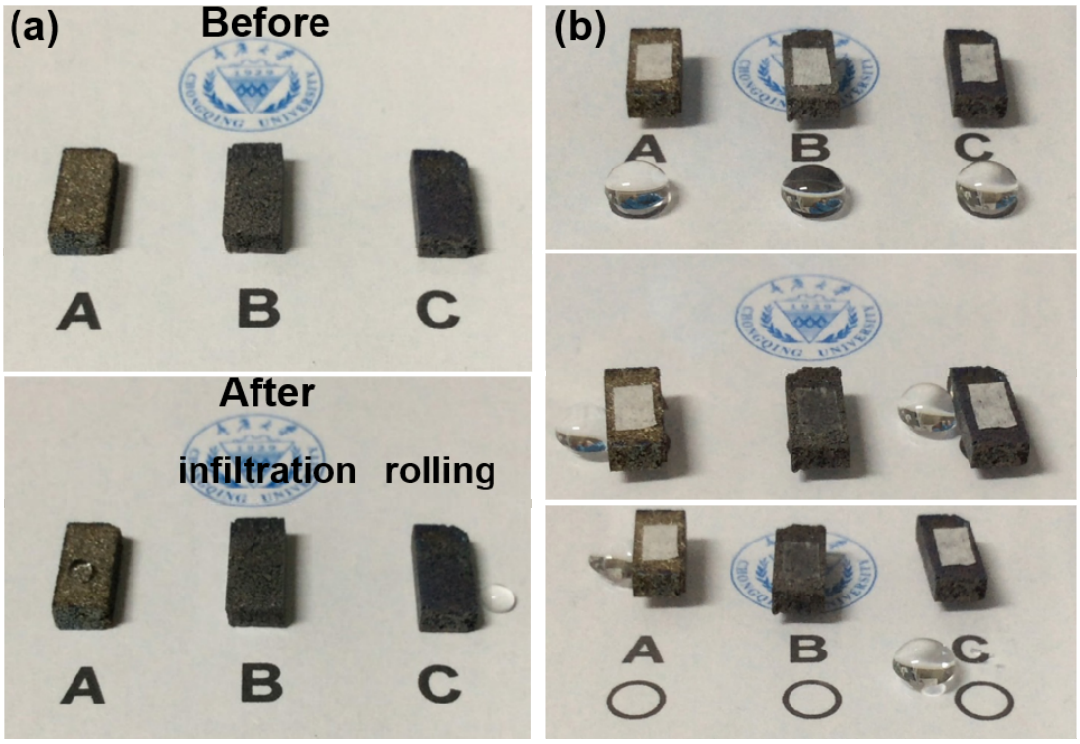

Figure S4. Surface wettability characteristics of different Ti foams, related to Figure 1. Demonstration of top-down infiltration (a) and bottom-up absorption (b) of water droplets for different Ti foams: A, original; B, superhydrophilic; C, superhydrophobic. A piece of filter paper was put on top of each foam in (b).

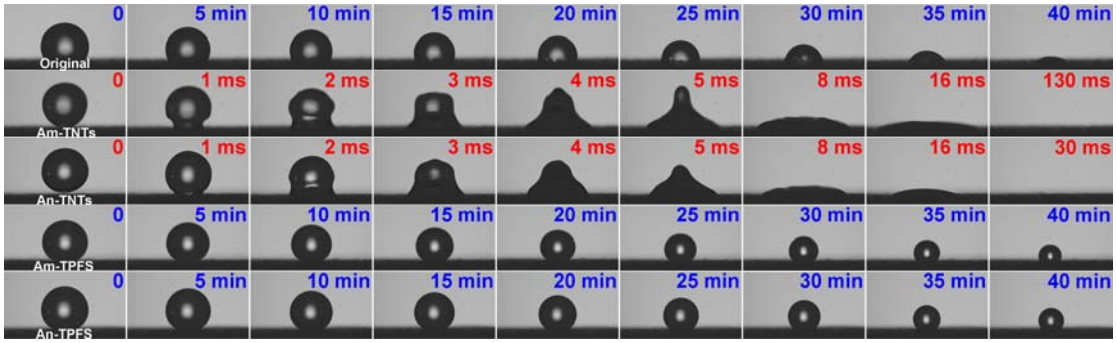

Figure S5. Water droplet evolution on different Ti foams, related to Figure 1. Time sequence of movie frames showing the evolution of water droplet on different foams in Table S1: Type-I (original, 1st row), Type-II (Am-TNTs, 2nd row), Type-III (An-TNTs, 3rd row), Type-IV (Am-TPFS, 4th row) and Type-V (An-TPFS, 5th row).

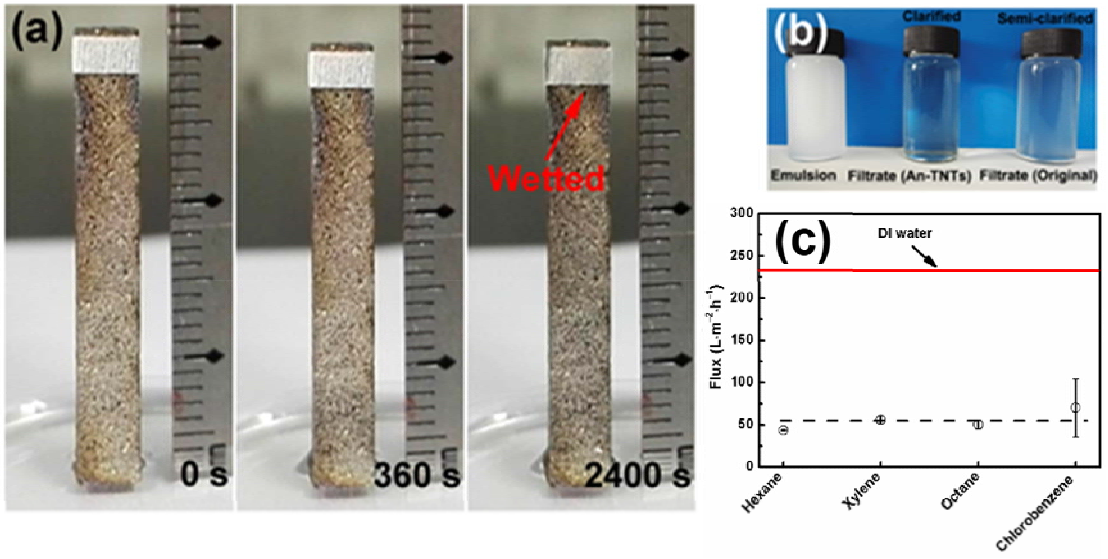

Figure S6. Water absorption effect of original Ti foam and oil-in-water emulsion separation performance of superhydrophilic foam, related to Figures 1 and 2. (a) Demonstration of bottom-up water absorption (capillary effect) for an original titanium foam of about 30 mm in height; the foam was in contact with water at the bottom and wrapped with filter paper at the top to detect the wetting height and speed by water; (b) Photographs of original octane-in-water emulsion (volume ratio 1:40) (left) and the filtrate obtained using superhydropilic (middle) and original (right) foams; (c) Infiltration capability of water and different emulsions using the setup in Figure 2 (see main text) with superhydrophilic foams.

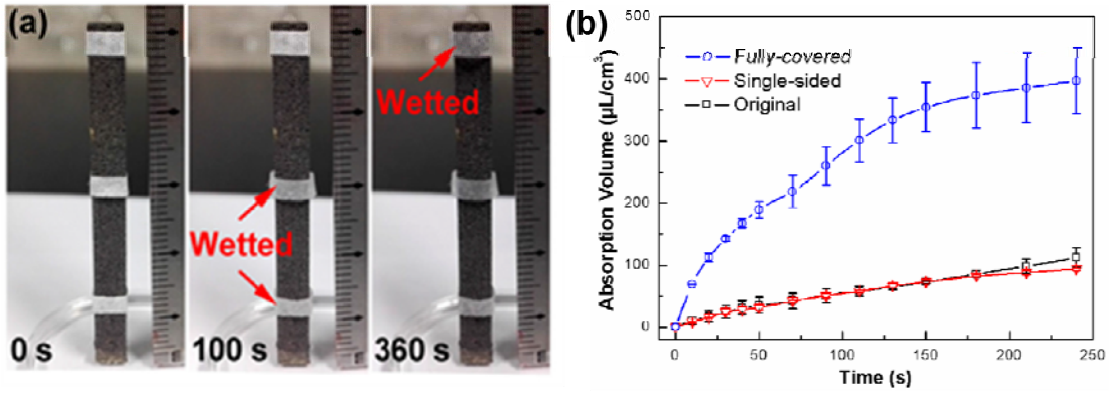

Figure S7. Water absorption property for different foams, related to Figure 1. (a) Demonstration of bottom-up water absorption for a superhydrophilic foam of about 50 mm in height; (b) the relation of absorption volume with time for the original foam (Original), the foam fully covered with nanotubes (Fully-covered), and the foam with only one surface layer being covered with nanotubes (Single-sided). See also Movie 4-5. For the Fully-covered foam (Type-II and Type-III), the water was instantaneously absorbed into the titanium foam and infiltrated to the upper surface under the capillary force, resulting in the wetting of the paper. As for the Original (Type-I) and Single-sided foams, the absorption process was extremely slow.

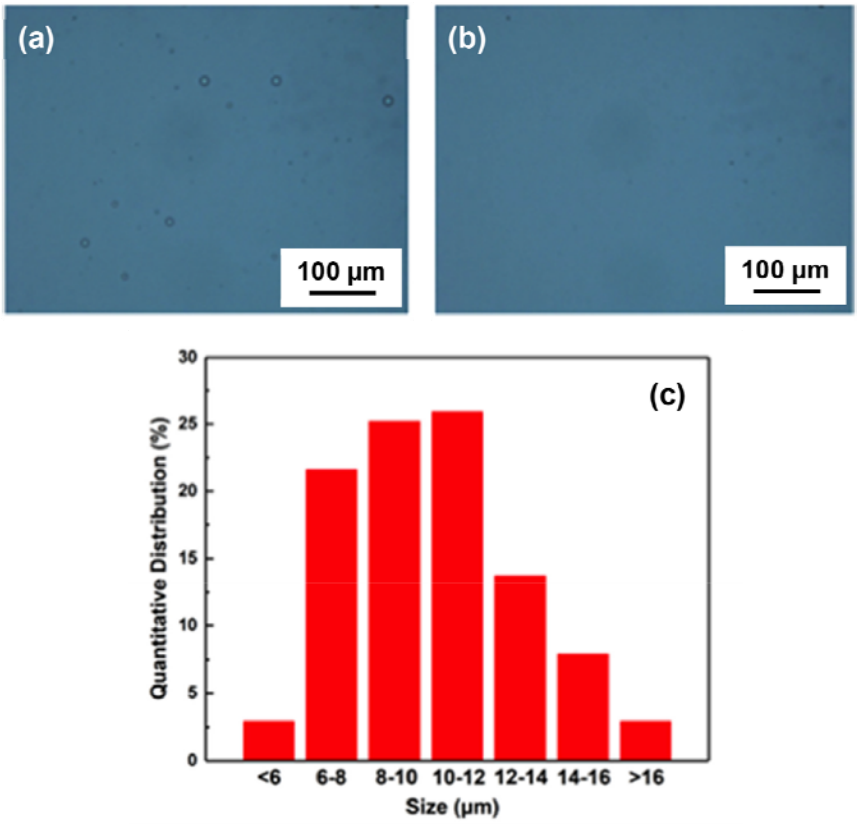

Figure S8. Oil droplet size in octane-in-water emulsion, related to Figure 2. Optical images of octane-in-water emulsions before (a) and after (b) filtration by superhydrophilic foams (Type-III). Corresponding statistics of the droplet diameter is given in (c).

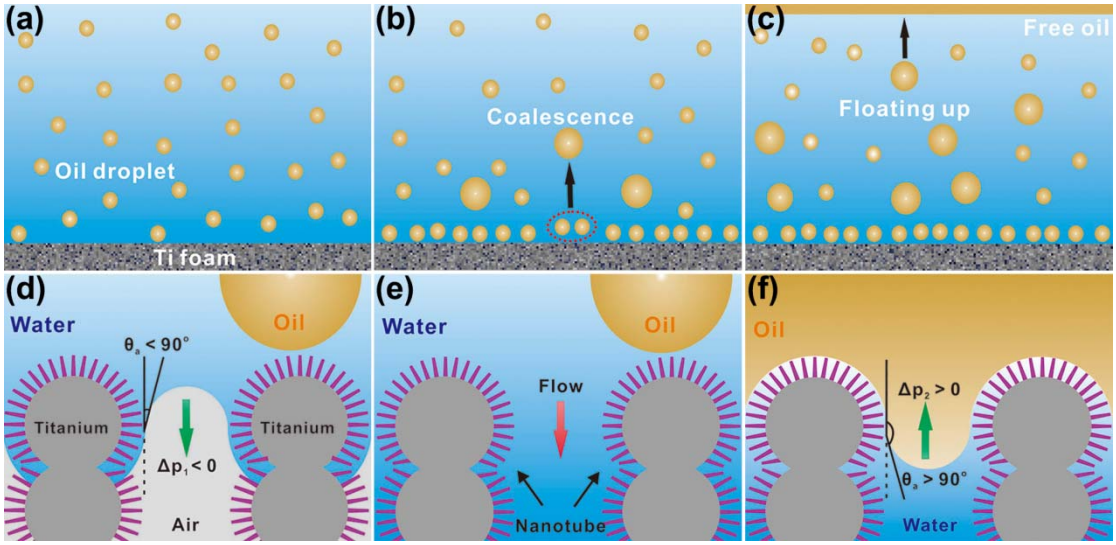

Figure S9. Demulsion mechanism, related to Figure 2. Illustration of the demulsion process (a-c) and the corresponding micromechanism (d-f) using superhydrophilic foams (Type-III).

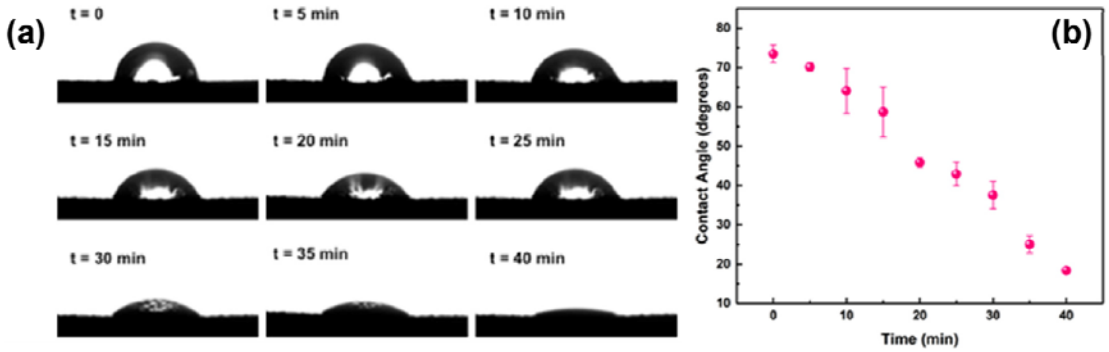

Figure S10. Evolution of water droplet on the single-sided foam, related to Figure 1. (a) Time sequence of movie frames showing the evolution of water droplet on the foam, with only one surface layer being covered with nanotubes (Single-sided); (b) Contact angle of the water droplet as a function of time for the foam tested in (a).

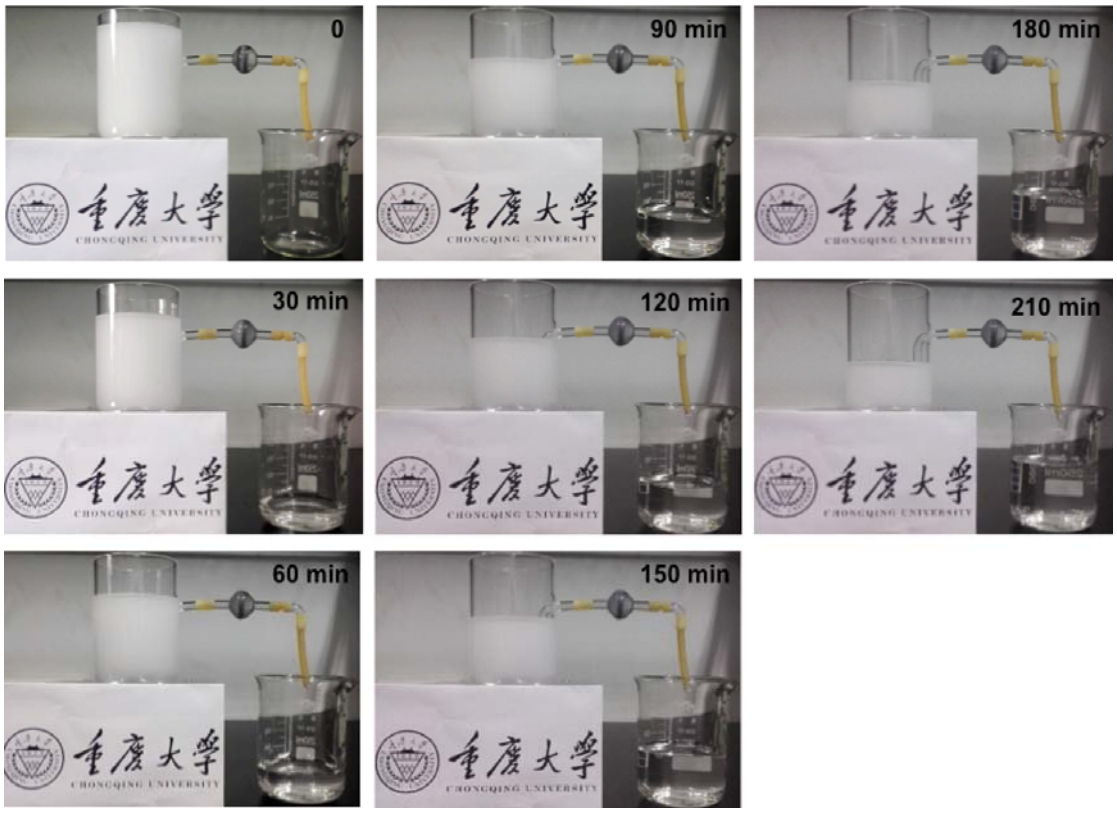

Figure S11. Siphon-like demulsificator for oil/water separation, related to Figure 3. Siphon test using the superhydrophilic foam (Type-III) coated with TiO_2 nanotube arrays in the 3D percolative channels, related to Fig. 3.

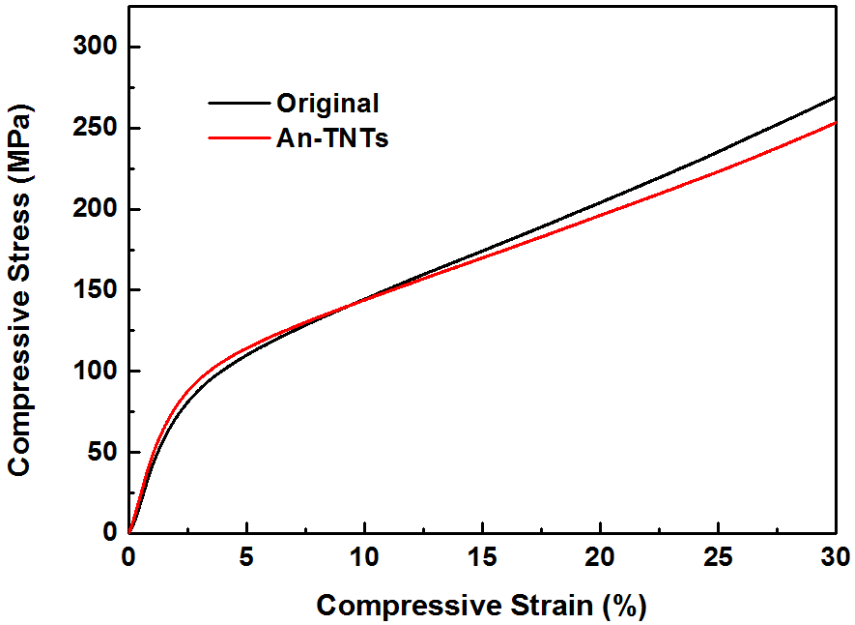

Figure S12. Mechanical properties of different foams, related to Figure 3. It is seen that the An-TNTs foam keeps almost the same mechanical properties as the original Ti foam, indicating that our demulsificator is of strong durability with respect to many such as organic oil-water separators.

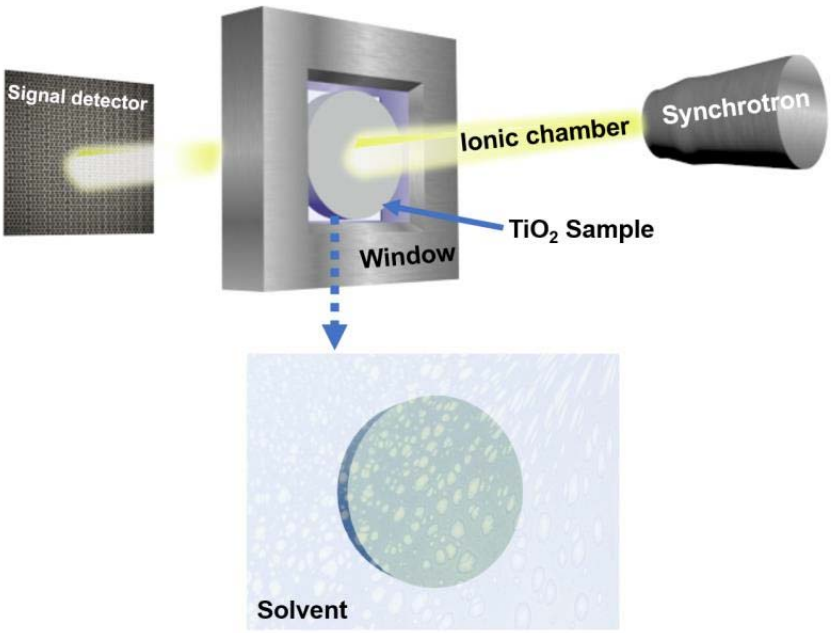

Figure S13. Experimental setup for in-situ XANES measurement, related to Figure 3. The samples were immersed in liquids during the measurement using a customized holder.

Table S1. Summarization of different Ti foams studied in this work, related to Figure 1

	Foam description	Wettability
Type-I	Original Ti foam	Hydrophobic
Type-II	Ti foam decorated with amorphous TNTAs	Superhydrophilic
Type-III	Ti foam decorated with anatase TNTAs	Superhydrophilic
Type-IV	Ti foam decorated with amorphous TNTAs and treated by TPFS	Superhydrophobic
Type-V	Ti foam decorated with anatase TNTAs and treated by TPFS	Superhydrophobic

Transparent Methods

Fabrication of 3D percolative superhydrophilic channels. Titanium foams (thickness: 3 mm, porosity: 38 vol%, accuracy: 30 μm) were ultrasonically cleaned in isopropanol, alcohol, sulfuric acid and deionized water for 15 min each, and finally dried in a nitrogen steam. The TiO_2 nanotube arrays were produced by anodizationin ethylene glycol (EG, anhydrous, 99.8%, Sigma-Aldrich) containing deionized water ($EG_{(wt)}/H_2O_{(wt)} = n$, n = 2, 4, 8, 16) and 0.3 wt% ammonium fluoride (NH_4F, 98%, ACS reagent, Sigma-Aldrich) under a constant voltage of 40 V (Kethley 2450 SourceMeter as the power supply) at room temperature (~22°C) for 40 min. A longer anodization durationwas employed in the electrolyte solution with n=4 to achieve open-ended TNTs. The resulting titanium foams were then annealed at 450°C for 3 h in furnace (LE140K1BN, Nabertherm) for crystallization. For superhydrophobic treatment, the foams were immersed in *n*-hexane (99%, Adamas) containing 0.5 vol% trichloro (1*H*, 1*H*, 2*H*, 2*H*-perfluorooctyl) silane (TPFS, 97%, Sigma-Aldrich) for 30 min, and then annealed in nitrogen atmosphere at 110°C for 1 h.

Characterizations of the TNT behaviors. The surface and cross-sectional morphologies of TNTs were examined by field-emission scanning electron microscope (FESEM, FEI Nova 400). The length of the nanotubes was directly determined by the ImageJ software. The evolutions of the sessile droplets on the foams were recorded by a high speed video camera. The initial volume of the droplet was about 5 μL. In absorption test, the foam (about 50 mm in height) fully covered with TNTs was in contact with water at the bottom. The absorption volume V_t ($\mu L \cdot cm^{-3}$) was determined by:

$$V_t = (w_t - w_0) / \rho V_0$$

where w_0 and V_0 are the weight and volume of the foam, w_t is the total weight of the foam after absorption for t min, and ρ is the water density.

Oil-in-water emulsion separation related methods. The resulting superhydrophilic foams were fixed between two quartz glass tubes. Four kinds of oils, including hexane (95%, anhydrous, Sigma-Aldrich), xylene (99%, anhydrous, Sigma-Alidrich), octane (99%, anhydrous, Sigma-Alidrich) and chlorobenzene (99.8%, anhydrous, Sigma-Alidrich), were applied for oil-in-water emulsion separation. All emulsions were prepared by ultrasonically mixing oil with water (volume ratio of 1/40) for 30 min. The emulsions were then poured into the upper tube, and the separation was only driven by gravity. After separation, the foam was washed with ethanol and dried in a vacuum oven at 50°C, and reused for recycling test. The filtrate water was collected for total organic carbon test (TOC, SSM-5000A, Shimazu). The separation efficiency was computed by oil rejection coefficient R, as follows (Xue et al., 2011):

$$R = [1 - (C_p / C_o)] \times 100\%$$

where C_o and C_p are the oil concentration of the original oil/water mixture and the collected water after one time separation, respectively.

Supplemental References

Xue, Z., Wang, S., Lin, L., Chen, L., Liu, M., Feng, L., and Jiang, L. (2011). A novel superhydrophilic and underwater superoleophobic hydrogel-coated mesh for oil/water separation. Adv. Mater. *23*, 4270-4273.